JGR Solid Earth

RESEARCH ARTICLE
10.1029/2020JB019524

Seismic Velocity Changes Caused by Water Table Fluctuation in the New Madrid Seismic Zone and Mississippi Embayment

Chunyu Liu[1], **Khurram Aslam**[1,2], **and Eric Daub**[1,3]

[1]Center for Earthquake Research and Information, University of Memphis, Memphis, TN, USA, [2]Department of Earth Sciences, University of Oregon, Eugene, OR, USA, [3]Alan Turing Institute, London, UK

Key Points:
- We observe the minimum wave speed from May to July due to the increased pore pressure from the water table fluctuation and the maximum wave speed in September/October
- The $\delta t/t$ correlates primarily with the water table fluctuation
- A poroelastic model can explain the velocity variations in the crust

Supporting Information:
- Supporting Information S1

Correspondence to:
C. Liu,
yclmq3@mst.edu

Citation:
Liu, C., Aslam, K., & Daub, E. (2020). Seismic velocity changes caused by water table fluctuation in the New Madrid seismic zone and Mississippi embayment. *Journal of Geophysical Research: Solid Earth*, *125*, e2020JB019524. https://doi.org/10.1029/2020JB019524

Received 3 FEB 2020
Accepted 27 JUL 2020
Accepted article online 29 JUL 2020

Abstract We use cross correlation of the ambient seismic field to estimate seasonal variations of seismic velocity in the Mississippi Embayment and to determine the underlying physical mechanisms. Our main observation is that the $\delta t/t$ variations correlate primarily with the water table fluctuation, with the largest positive value from May to July and the largest negative value in September/October relative to the annual mean. The $\delta v/v$ residuals after water level fluctuation correction correlate with air pressure in the short term and follow the trend of temperature in the long term. The $\delta v/v$ residuals after water level fluctuation and air pressure correction correlate inversely with the wind speed. The correlation coefficients between water table fluctuation and $\delta t/t$ are independent of the interstation distance and frequency, but high coefficients are observed more often between 0.3 and 1 Hz than between 1 and 2 Hz because high-frequency coherent signals attenuate faster than low-frequency ones. The $\delta t/t$ variations lag behind the water table fluctuation by about 20 days, which suggests that the velocity changes can be attributed to the pore pressure diffusion effect. The seasonal variations of $\delta t/t$ are azimuthally independent, and a large increase of noise amplitude only introduces a small increase to the $\delta t/t$ variation. At close distances, the maximum $\delta t/t$ holds a wide range of values, which is likely related to local structure. At larger distances, velocity variations sample a larger region so that it stabilizes to a more uniform value. We find that the observed changes in wave speed can be explained by a poroelastic model.

1. Introduction

Extensive field and laboratory studies have been dedicated to understanding the crustal responses including seismic velocity variations and subsurface strain changes due to the internal tectonic and external climatological stress loadings (Ben-Zion & Allam, 2013; Ben-Zion & Leary, 1986; De Fazio et al., 1973; Hadziioannou et al., 2009; Hillers et al., 2015; Meier et al., 2010; Sens-Schönfelder & Larose, 2008; Wu et al., 2016). Monitoring the crustal response can not only track the evolving stress and constrain the effective rheology with depth but also help to understand the crustal response to the internal tectonic stress by removing the response to the climatological stress loadings (Hillers et al., 2015; Rivet et al., 2015; Wang et al., 2017). Because different rocks or structures respond differently to the internal and external loadings, monitoring the crustal response can also help to identify local structure anomalies and understand wave propagation and attenuation (Wang et al., 2017). More specifically, measurements of the temporal changes of seismic velocity can shed light on the fault zone coseismic damage and postseismic healing (Brenguier et al., 2008; Liu, Huang, et al., 2018; Wu, 2016), volcanic eruption early warning (Brenguier et al., 2008; Duputel et al., 2009), groundwater levels (Clements & Denolle, 2018; Lecocq et al., 2017), climatological parameters such as precipitation (Sens-Schönfelder & Wegler, 2006), temperature (Meier et al., 2010; Sens-Schönfelder & Larose, 2008), and atmospheric pressure (Niu et al., 2008; Silver et al., 2007), solid earth tidal (De Fazio et al., 1973; Mao et al., 2019) and oceanic tidal deformation (Hillers et al., 2015; Yamamura et al., 2003), and instrumental errors (Stehly et al., 2007; Sens-Schönfelder, 2008). Taking advantage of long-term dense seismic station deployments, a systematic investigation of seismic velocity variation can improve our understanding of the crustal response to the climatological loadings.

The Mississippi embayment (ME) (Figure 1) is a SSW plunging trough filled with late Cretaceous and Cenozoic sediments that can reach a thickness of ≈1.5 km (Dart, 1992; Dart & Swolfs, 1998; Hildenbrand & Hendricks, 1995). The ME has experienced long-term and complicated geological activities including

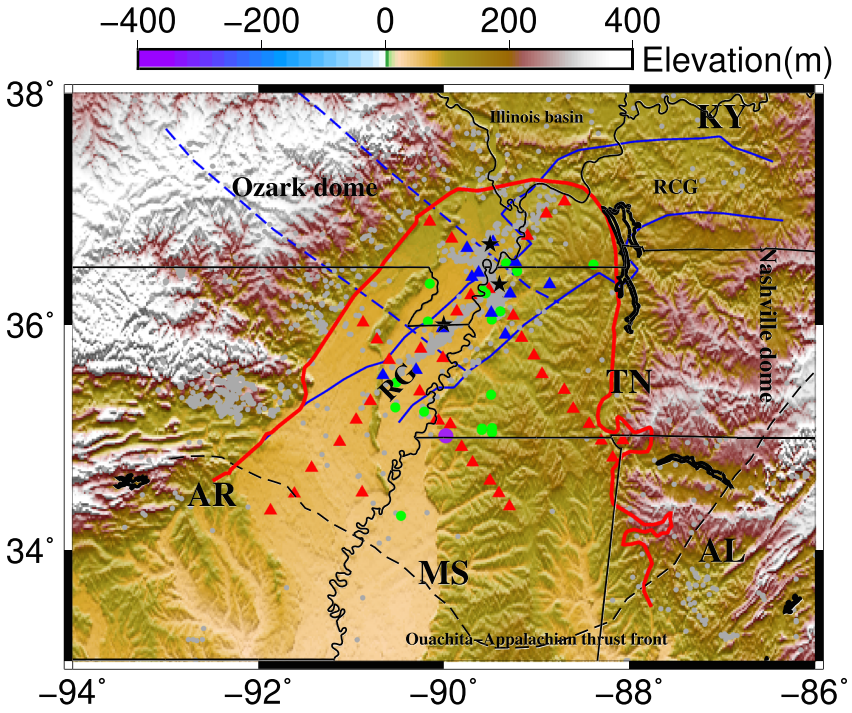

Figure 1. Index map of the Mississippi embayment in the central United States showing $M_w > 2.0$ earthquake catalog from 1990 to 2018 (small gray dots), three $M_w > 7.0$ earthquakes (black stars), broadband stations (red triangles) used for cross correlations (CCs) in 2014, stations used for computation of CCs from 2010 to 2018 (blue triangles), groundwater site stations (green circles), temperature, air pressure, and wind speed monitoring site (purple circle), Reelfoot-Rough Creek graben (RG-RCG, blue solid lines) and Missouri Batholith (blue dashed lines) modified from Hildenbrand and Hendricks (1995), sediment boundaries of Mississippi embayment (red solid lines) modified from Dart (1992) and Dart and Swolfs (1998), Ouachita-Appalachian thrust front (black dashed lines), Nashville dome, and Ozark dome. From southwest to northeast, three major earthquakes occurred on 16 December 1811 with $M_w = 7.7$, 23 January 1812 with $M_w = 7.5$, and 7 February 1812 with $M_w = 7.7$.

uplift, rifting, and subsidence and has hosted three $M_w > 7.0$ earthquakes (Figure 1) that occurred in the winter of 1811–1812 (Johnston & Schweig, 1996). We target the ME for two reasons. First, long-term continuous monitoring and dense broadband station distribution allow us to conduct a thorough temporal velocity investigation which may provide insight into how the climatological parameters influence the seismic velocity. Second, few studies of this type have been done in intraplate fault zones, so such an investigation can help us understand if there are significant differences between interplate and intraplate fault zones and how they respond to external changes in forcing.

Estimating seismic velocity change has been done by measuring the travel time or phase difference from active sources including explosions (Li et al., 1998, 2003, 2006; Nishimura et al., 2000), airguns (Wang et al., 2020; Wegler et al., 2006), and repeating earthquakes (Peng & Ben-Zion, 2006; Poupinet et al., 1984; Rubinstein & Beroza, 2004a, 2004b; Rubinstein et al., 2007; Schaff & Beroza, 2004), and by computing the dephasing of the ambient noise cross correlations (CCs) (Brenguier et al., 2008; Sens-Schönfelder & Wegler, 2006) or autocorrelations (ACs) (Minato et al., 2012; Ohmi et al., 2008). We prefer ambient noise analysis because it not only circumvents the uncertainty of repeating earthquakes and high expense of the active sources but also allows for long-term velocity monitoring over time periods of months to years. The CCs of the ambient noise can effectively retrieve empirical Green's function between a pair of stations (Derode et al., 2003; Sabra et al., 2005; Shapiro & Campillo, 2004; R. L. Weaver & Lobkis, 2001). The dephasing of scattered waves in daily CCs relative to those in a reference CC reflects the temporal change of the elastic behavior of the crust.

We apply ambient noise CCs to all broadband seismic stations inside the ME over four frequency ranges and investigate temporal variations of seismic velocity and correlation with the climatological parameters. We compare the calculated seismic velocity variation of each station pair with the regional climatological

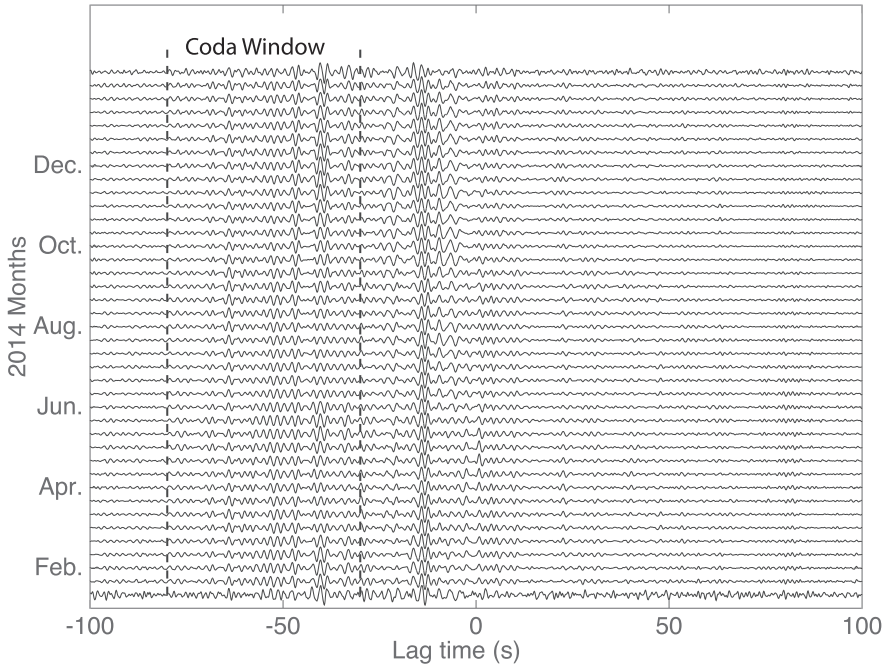

Figure 2. Example of 30 days moving stacked vertical component CCs for the station pair C07:C08 of the network NELE in 2014. The interstation distance is 30 km. The CCs are in the passband of 0.3–1 Hz. The dashed lines from −80 to −30 s mark the coda window.

parameters to investigate the possible mechanisms for the velocity changes. We address the following questions: What are the physical mechanisms behind the temporal velocity changes in the ME? Do the maximum velocity variations depend on characteristics of the waves, such as the interstation distance and azimuth? What are the correlation coefficients of velocity changes with the climatological parameter variations? The cross-correlation methods applied to the data from the ME give us a unique view into the physical mechanisms behind changes in seismic velocity over time and how the changes are related to the nontectonic effects that may complicate the analysis of more active tectonic regions.

2. Data and Analysis Procedure

The installation of Northern Embayment Lithosphere Experiment (NELE) with large aperture and continuous recording in 2014 enables us to investigate the temporal variations of seismic velocity. We use 53 broadband stations (Figure 1) to compute the CCs. All broadband stations are inside the ME as can be seen by comparing station locations to the sediment thickness contours. Because sediment-influenced waves may better reflect the sediment elastic behavior than the direct crustal surface wave arrivals, we limit the interstation distance to at most 100 km where Langston et al. (2005) and Liu et al. (2019) observed direct sedimentary surface wave arrivals in the passband of 0.2–1.5 Hz. In order to investigate the annual temporal variations, we only use stations which have a continuous full-year recording in 2014. Finally, we compute 373 velocity variations for all station pairs in 2014 to investigate how they behave seasonally.

We follow the analysis procedure of Brenguier et al. (2008) and Lecocq et al. (2014) in this study. We download continuous daily vertical component miniseed data from IRIS (www.iris.edu) by the FDSN web service and use the MSNoise Python package (Lecocq et al., 2014) to compute the CCs. The data processing details are available in Lecocq et al. (2014) and are described briefly here. For each station pair, we first scan yearly data into MSNoise, downsample to 10 Hz, and remove instrument response. We also remove earthquakes by the root-mean-square (RMS) temporal normalization and reduce the effect of nonuniform source distributions by spectral whitening. Langston et al. (2009) and Liu, Langston, et al., (2018) observed the major oceanic-generated ambient noise in the frequency range of 0.02–0.33 Hz in the ME, and sedimentary surface waves emerge in the passband of 0.2–1.5 Hz (Langston et al., 2005; Liu et al., 2019). Considering that the

dominant frequency range of waves scattered by sediments is higher than that of the oceanic ambient noise (Liu et al., 2019), we define four frequency ranges: 0.3–1, 0.5–1.2, 0.7–1.5, and 1–2 Hz. Because Rayleigh waves have peak sensitivity to the shear wave velocity changes at the depth of one third of a wavelength, scattered waves with a period of 3 s and phase velocity of 1.7 km/s (Dorman & Smalley, 1994) can be sensitive to velocity changes at depths up to 1.7 km. We construct a monthly CC through stacking the past 30 days CCs from the selected date and average all daily CCs to obtain the reference CC. We use a moving-window cross-spectral (MWCS) method (Clarke et al., 2011; Poupinet et al., 1984) to measure the relative dephasing between monthly moving stack CCs and yearly reference CC, as Zhan et al. (2013) suggested that the stretching method (Wegler & Sens-Schönfelder, 2007) can cause apparent velocity changes due to changes in the amplitude and phase spectrum. The MWCS measures the arrival time difference between two windowed waveforms by computing cross coherency between energy densities in the frequency domain. Linear regression of time differences over moving coda windows constrains the fractional change in travel time $\delta t/t$. The errors of $\delta t/t$ are estimated using the cross coherency and the squared misfit to the linear regression slope (Clarke et al., 2011). The velocity change ($\delta v/v$) is deduced by the relationship $\delta v/v = -\delta t/t$, which assumes that $\delta v/v$ is spatially homogeneous. A coda window defined for the MWCS is shown in Figure 2. We define the coda window based on the timing of large-amplitude scattered wave arrivals (group velocity <1.0 km/s) in the monthly moving stack CCs (Figure 2).

The velocity variations are known to be associated with climatological parameters such as water table height, precipitation, temperature, atmospheric pressure, and wind speed (Hillers et al., 2015; Meier et al., 2010; Sens-Schönfelder & Larose, 2008; Sens-Schönfelder & Wegler, 2006). We obtain daily water table data of 19 stations from the USGS water information system and precipitation, temperature, atmospheric pressure, and wind speed from the National Oceanic and Atmospheric Administration (NOAA)(Figure 1). We calculate the water table fluctuation by subtracting the daily water table from the maximum water table over 1 year. We observe similar amplitude and consistent phase for the water table fluctuation of most stations. A few locations exhibit larger amplitude variations consistently over time, suggesting they reflect local structure rather than differences in precipitation. Because the velocity variations have a different dependence on the changes of the climatological parameters, we remove the mean and normalize the maximum of the absolute value of the velocity variations, water table fluctuation, precipitation, temperature, atmospheric pressure, and wind speed to unity for comparison.

3. Analysis of Seismic Velocity Variations

We measure yearly $\delta t/t$ variations for all 373 station pairs over four predefined frequency ranges in 2014. The CCs for all station pairs are computed in the passband of 0.3–2 Hz, and the MWCS and $\delta t/t$ variations are determined in predefined frequency ranges. The $\delta t/t$ increases to its maximum in May and June and decreases to its minimum in September and October relative to the average (Figure 3). The $\delta t/t$ variations correlate primarily with the normalized water table fluctuation in the four predefined frequency ranges. We select 205, 198, 158, and 96 $\delta t/t$ variations in the passbands of 0.3–1, 0.5–1.2, 0.7–1.5, and 1–2 Hz based on two criteria: (1) The correlation coefficient with the normalized water table fluctuation is higher than 0.3, and 2) they show seasonal variation. That is, the wave speed is slower than average in late spring to summer and is faster in late fall to early winter. If we cannot observe a seasonal variation of $\delta t/t$, estimation of maximum $\delta t/t$ cannot be correctly determined. We determine the maximum $\delta t/t$ for each station pair by smoothing the $\delta t/t$ over the entire year with a 10-day moving average window and compute the maximum of the smoothed variations, which removes spurious velocity variations with large errors. In the following sections, we evaluate how the $\delta t/t$ and correlation coefficients vary in different frequency ranges, how the maximum $\delta t/t$ and correlation coefficients depend on the characteristics of the waves, such as interstation distance and azimuth.

3.1. Correlation With the Climatological Parameters

Climatological loadings can induce various crustal responses including stress/strain changes (Ben-Zion & Allam, 2013), earthquake triggering (Husen et al., 2007; Liu et al., 2009), and seismic velocity variations (Hillers et al., 2015; Meier et al., 2010). The precipitation/water table fluctuation, atmospheric pressure, and wind speed influence the elastic stress by changing the pore pressure or water saturation, air pressure redistribution, and wind on contact shearing, respectively. The temperature has an impact on regional

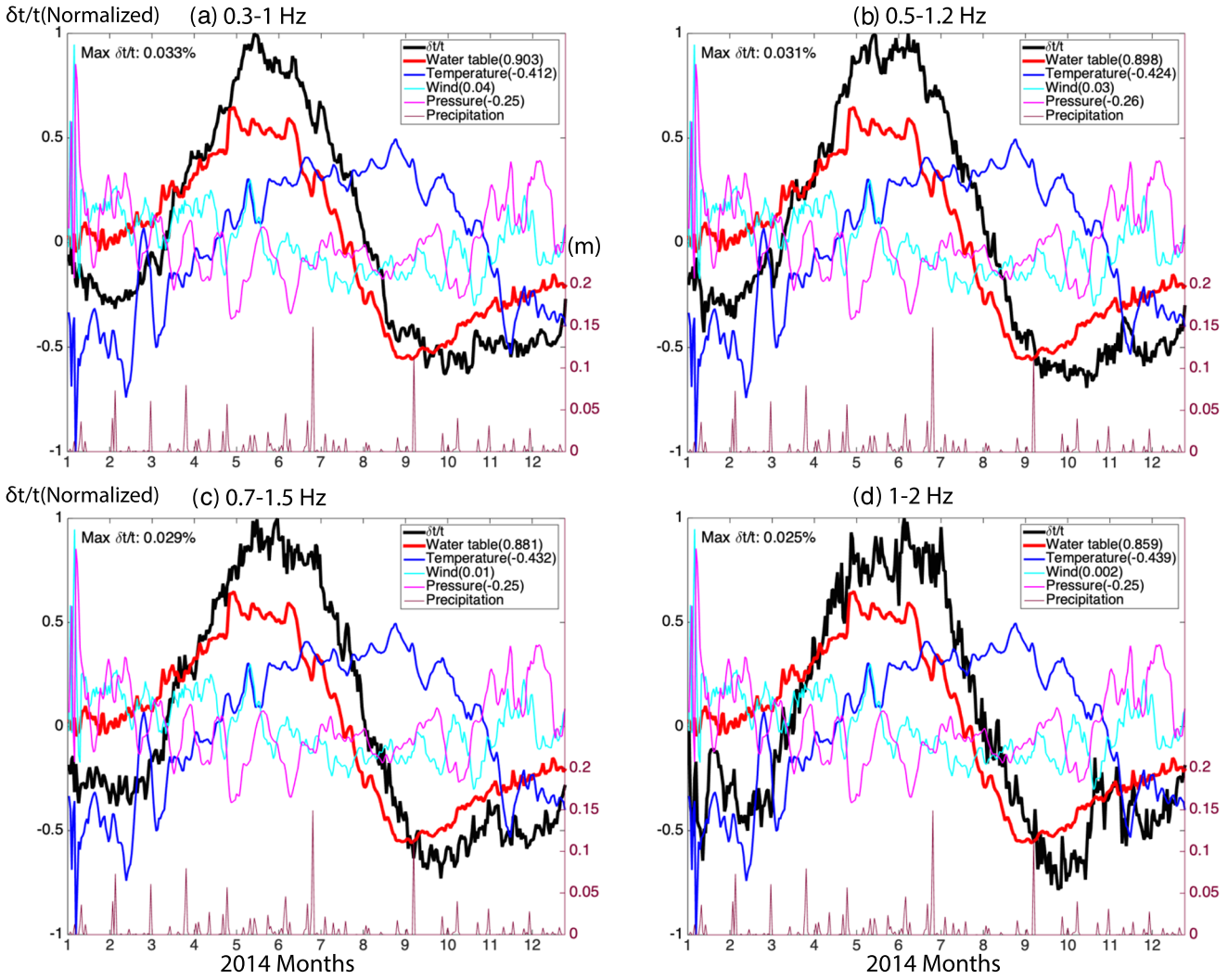

Figure 3. The correlation of averaged normalized $\delta t/t$ for all station pairs with normalized climatological parameters, water table fluctuation, precipitation, temperature, wind speed, and atmospheric pressure, in the passbands from (a) 0.3–1, (b) 0.5–1.2, (c) 0.7–1.5, and (d) 1–2 Hz. The right-side vertical scale is for the precipitation. The values after the climatological parameters in the legend represent the correlation coefficients with the $\delta t/t$. The observed value of $\delta t/t$ correlates primarily with the normalized water table fluctuation in all predefined frequency ranges.

thermoelastic stress because of thermal expansion or contraction due to ambient temperature changes. The elastic and thermoelastic stress changes directly affect the strain field, which can be used to model the seismic velocity variations (Rivet et al., 2015; Tsai, 2011; Wang et al., 2017).

The magnitude of the velocity variations and their dependence on the climatological parameters vary throughout the world. Sens-Schönfelder and Wegler (2006) observed that $\delta v/v$ varies seasonally with an amplitude of 0.02% in the frequency band >0.5 Hz at Merapi volcano, Indonesia, and suggested that the variation is due to changes of the water table. Wang et al. (2017) observed up to a 0.02% velocity variation in the passband of 0.15–0.9 Hz using data from 2011 to 2012 throughout Japan and proposed that the velocity variations could be due to different effects including pore pressure, snow depth, and sea level changes for different regions. Ben-Zion and Leary (1986) suggested that the temperature could cause an effect 10 times larger than water table fluctuations around 15 m. Meier et al. (2010) observed a maximum 0.1% velocity change in the 0.1–2 Hz passband using data from 2001 to 2004 in the Los Angeles basin, and suggested that it was associated with the thermoelastic strain variation. These studies indicate that the velocity variations could be associated with different climatological parameters, and maximum velocity variations induced by temperature could be higher than that caused by water table fluctuations.

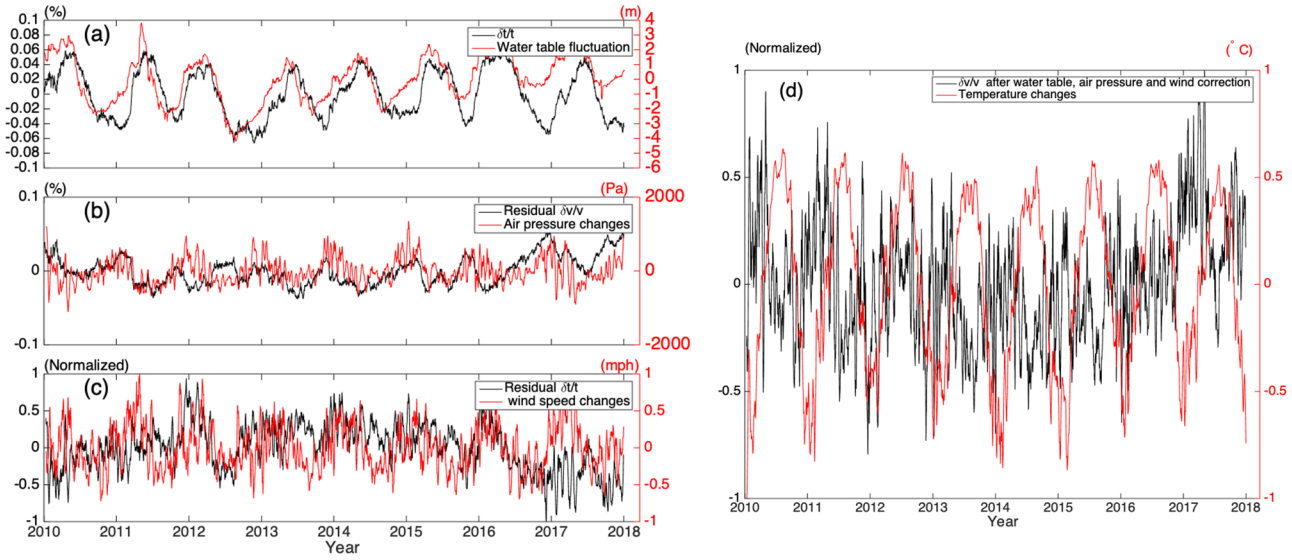

Figure 4. Analysis of the correlation of normalized seismic velocity variation with climatological parameters. Seismic velocity changes correlate primarily with water table fluctuation. (a) The $\delta v/v$ residuals after water table fluctuation correction (including the diffusion effect) correlate positively with air pressure. The $\delta v/v$ residuals after water table and air pressure correction are shown in (b) and (c), respectively. (d) The $\delta v/v$ residuals after water table fluctuation, air pressure, and wind correction follow the trend of temperature in the long term, which shows a slight decrease and then an increase. Ben-Zion and Leary (1986) found that the temperature is positively correlated with the $\delta v/v$. Niu et al. (2008) observed that air pressure is positively correlated with the $\delta v/v$. Sens-Schönfelder and Wegler (2006) and Wang et al. (2017) observed that water table fluctuation is positively correlated with the $\delta t/t$. To better observe amplitude and phase correlation between velocity changes and variations of climatological parameters, we use $\delta t/t$ to compare with the water table fluctuation and wind speed but $\delta v/v$ with air pressure and temperature. Note that all climatological parameters are shown relative to average in the figures.

Determining the most strongly correlated parameter with velocity variation can help us understand the dominant mechanisms driving the velocity changes for the ME. In Figure 3, we show the correlations between the normalized average $\delta t/t$ for all station pairs and the normalized precipitation, water table fluctuation, temperature, atmospheric pressure, and wind speed in four predefined frequency ranges. The $\delta t/t$ correlates most strongly with the normalized water table fluctuation.

We also compute seasonal variations of velocity (Figure 4) for 43 pairs of stations (Figure 1) from 2010 to 2018 to investigate the long-term variation. The $\delta t/t$ variations are strongly correlated with the water table fluctuation with error around 0.01% (Figure S2 in the supporting information). In the short term, the $\delta v/v$ residuals after water table fluctuation correction correlate with air pressure. Niu et al. (2008) observed that an increase of air pressure can increase seismic velocity. The $\delta t/t_{syn}$ residuals after water table fluctuation and air pressure correction correlate with the wind speed. Wind speed changes are not considered to be responsible for $\delta t/t$ variation but may cause systematic noise excitation, which introduces a bias to the $\delta t/t$ measurement (Hillers et al., 2015). In the long term, the $\delta v/v$ residuals show a slight decrease and then an increase from 2010 to 2018 and follow the trend of temperature variation (Lecocq et al., 2017). Tsai (2011) and Ben-Zion and Leary (1986) also found that the temperature is positively correlated with the $\delta v/v$. Comparing pressures induced from different climatological parameters (Brekke, 1959; Tsai, 2011), we also find that pore pressure change is greater than wind pressure and air pressure changes (see supporting information text and Figure S3). How the climatological parameters interact with each other and if that interaction could affect the velocity variation is not considered in this study.

The strong correlation between $\delta t/t$ and the water table fluctuation could be due to two possible effects. The water table fluctuation can affect the direct hydrological and poroelastic strain, which are related to the direct water loading and water diffusion effect, respectively. The maximum velocity variations due to the direct hydrological elastic or poroelastic strain changes are around 0.04% for the Los Angeles basin (Tsai, 2011). With similar sedimentary rock types and a few meters fluctuation in the water table (Figure S1), we might expect a similar magnitude of velocity variation for the ME. Direct water loading can affect hydrological strain instantaneously, but water diffusion usually takes some time to influence poroelastic strain.

Direct water loading increases $\delta v/v$ through an increase of water saturation at shallow depth while water diffusion increases pore pressure and decreases the area of grain contact, which decreases $\delta v/v$ at deeper levels. The $\delta t/t$ changes show a delay of 20 days relative to the normalized water table fluctuation based on when the maximum and minimum values occur (Figures 3 and 4). Our observations suggest that the water diffusion effect is the dominant mechanism for the velocity changes.

3.2. Poroelastic Physical Models for Seismic Velocity Changes

To facilitate our understanding of the dominant mechanism in the ME, we use a poroelastic physical model to estimate seasonal velocity variations from 2010 to 2018. Talwani et al. (2007) presented a solution for the one-dimensional fully coupled diffusion equation, which was later used for monitoring velocity changes by Rivet et al. (2015) and Wang et al. (2017). We consider pore pressure changes due to diffusion in the vertical direction and assume constant hydraulic diffusivity and density. The pore pressure changes $P(h,t)$ at h kilometer depth from the surface and on day t is

$$P(h,\ t) = \sum_{i=1}^{n} \delta p_i \ \mathrm{erfc}\left[\frac{h}{\sqrt{4c(n-i)\delta t}}\right], \tag{1}$$

in which n is the number of time increments δt from the day of the rainfall to the time t; δp_i is the groundwater load changes ($\rho \cdot g \cdot \delta h_i$) at the sampled instant $t_i = i\delta t$, and we obtain δh_i by averaging the groundwater level at 19 monitoring stations throughout the ME shown in Figure S1 and taking the change relative to the previous day. δt is set to 1 day, erfc[·] is the complementary error function, and c is the hydraulic diffusivity. The depth h is set to 1.7 km, which coincides to the depth sensitivity of surface waves in the frequency band 0.3–1 Hz. We use a transfer function approach from Rivet et al. (2015) and Wang et al. (2017) to model seismic velocity changes:

$$\frac{\delta v}{v}_{syn}(t) = \langle \frac{\delta v}{v}(t) \rangle + \frac{\mathrm{cov}(\frac{\delta v}{v}(t),\ P(t))}{\mathrm{var}(P(t))} * (P(t) - \langle P(t) \rangle), \tag{2}$$

where $\langle \cdot \rangle$ is the average over the entire time series. Talwani et al. (2007) suggested that the diffusion rate ranges from 0.1 to 10 m^2/s. We find the optimal c value of 2.0 m^2/s (Figure 5) through minimizing the squared residuals $\sigma^2(c)$:

$$\sigma^2(c) = \frac{1}{n}\sum_{t=1}^{n}\left(\frac{\delta v}{v}(t) - \frac{\delta v}{v}_{syn}(t,\ c)\right)^2, \tag{3}$$

where n is number of days. The modeled $\delta t/t$ correlates well with the observed one (Figure 5). However, we note that the observed and synthetic $\delta v/v$ signals still exhibit a small time lag between them (the cross correlation between these signals is maximized with a time lag of 8 days). This is due to the large residuals between the observed and synthetic velocity changes from 2016 to 2018, which as discussed above may be related to temperature effects not accounted for by this model. In this case, a larger value of the diffusivity increases the amplitude of the $\delta v/v$ variations, at the expense of a slightly worse time alignment between the signals. Thus, we also fit the diffusivity by minimizing the cross-correlation time lag between the signals, which gives an optimal diffisivity of 0.87 m^2/s (Figure 5). These comparisons show that reasonable values of c are able to reproduce the time dependence of the observed seismic velocity changes.

While the above approach captures the temporal relationship between the $\delta v/v$ observations and pore pressure, the transfer function approach is based on an empirical statistical correlation between the time series (note that one must know the observed $\delta v/v$ in order to compute the synthetic one in Equation 2) and does not assess if the magnitude of the velocity changes are physically reasonable given the pore pressure estimates and typical material properties. To address this, we also apply a simplified poroelastic solution (see supporting information text and Figure S4) from Tsai (2011) to estimate the magnitude of the seasonal variation of seismic velocity. With experimental Biot-Willis coefficient (Biot & Willis, 1957; Hart, 2000) and Poisson's ratio (Catchings, 1999) for sandstone, we estimate that an approximate m/μ (μ is the second Lamé constant and m is the Murnaghan constant Hughes & Kelly, 1953; Murnaghan, 1951) value

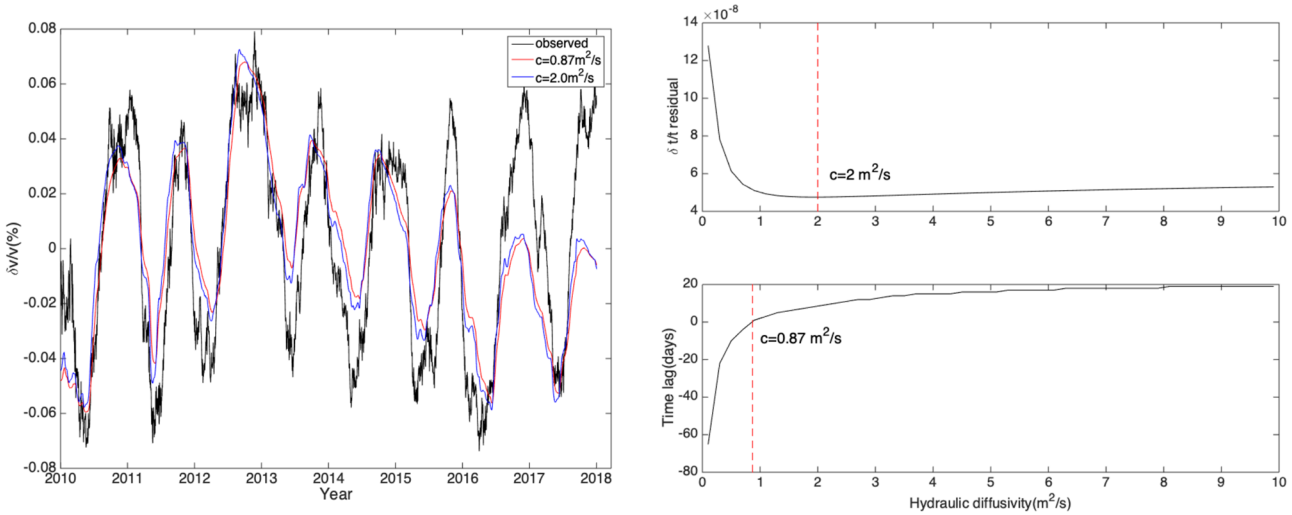

Figure 5. (left) Comparison of modeled and observed $\delta t/t$ from the pore pressure diffusion model. We compute the pore pressure loading at the surface from differentiation of the water table fluctuation and use a diffusion model to compute the velocity change at a depth of 1.7 km. The diffusivity values shown are found based on (top right) minimizing the squared residuals between the observed and synthetic $\delta t/t$ (2.0 m^2/s), or by (bottom right) minimizing the time lag where the cross correlation between the two time series is maximized (0.87 m^2/s).

required to match the modeled $\delta v/v$ with the observed one is −2000. It is in the range of values from experimental measurements (D'Angelo et al., 2008). However, the simplified model assumes a sinusoidal form for the pore pressure variation rather than computing it directly from water table variations.

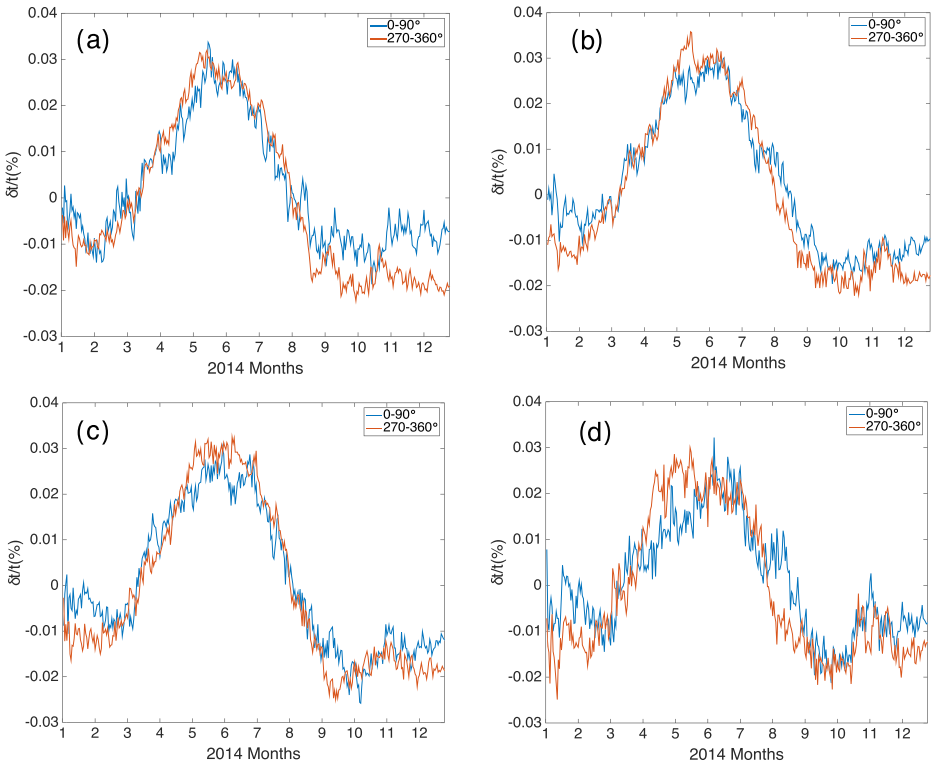

Figure 6. The $\delta t/t$ dependence on the azimuth in the passband of 0.3–1, 0.5–1.2, 0.7–1.5, and 1–2 Hz. Average $\delta t/t$ variations in the azimuth of 0–90° and 270–360° are similar to each other, and the differences between them are small. The nonuniform distribution of noise sources has a small effect on the $\delta t/t$ variations.

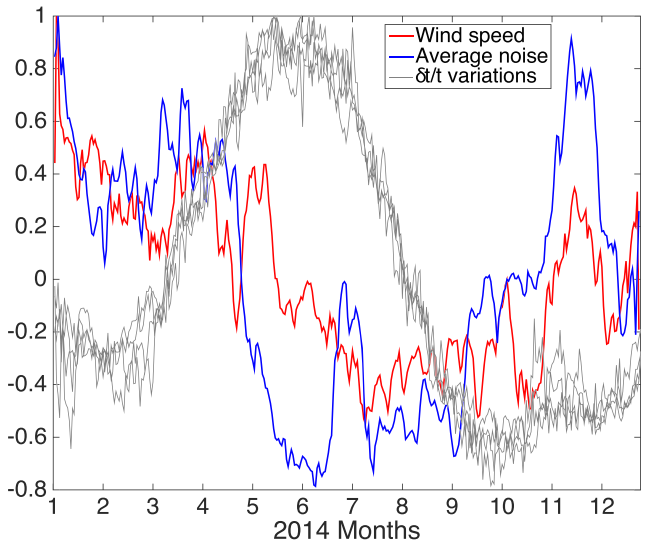

Figure 7. The $\delta t/t$ dependence on the seasonal variation of noise amplitude. High similarity, though not an exact match, can be observed between seasonal variation of noise amplitude and wind speed, which suggests that the noise in the passband of 0.3–2 Hz could be composed of oceanic microseisms, induced surface waves, and wind noise. High similarity can be observed between the variations of noise amplitude and $\delta t/t$ from January to April and October to December. A large increase of noise amplitude induces a small increase of $\delta t/t$ in November, which suggests that noise amplitude may introduce a small bias into the velocity measurements. The bias from noise amplitude variation is small compared to the maximum velocity change induced from the water table fluctuation from April to September. We suggest that the velocity variations are primarily related to the pore pressure changes in the crust or sediments, rather than the seasonal variations of the ambient noise amplitude.

Because of this assumption, the simplified model cannot capture the yearly differences in the amplitude and phase of the velocity changes.

3.3. The $\delta t/t$ Dependence on the Interstation Azimuth and Noise Amplitude

Seasonal variation of seismic velocity can reflect changes in material properties or be induced by seasonal changes of noise amplitude (Hillers et al., 2015). Heterogeneous distributions of the noise source can bias the estimation of arrival time (Froment et al., 2010; R. Weaver et al., 2009). Thus, a long-term change in the noise source distribution over several months can also be the cause of spurious seismic velocity changes.

Sources of microseisms usually distribute nonuniformly in different seasons (Langston et al., 2009; Liu et al., 2019; Tian & Ritzwoller, 2015; Young, 1999). However, scattering by local structures can randomize propagation directions and increase isotropy. In the ME, Liu et al. (2019) suggested that the generation of sedimentary surface waves in the passband of 0.2–1 Hz might be related to the basin edges. In the coda window, scattered waves (group velocity <1 km/s) can be composed of sedimentary surface waves (group velocity 0.7 m/s). In order to investigate if the velocity variations are azimuthally dependent, we compare the average velocity variations using station pairs with different azimuths. We initially do not differentiate the positive and negative lags of the CCs while calculating the $\delta t/t$ variations, so the propagation direction of scattered waves corresponding to the $\delta t/t$ estimation is uncertain. Because the edge of the ME surrounds the stations on the northwest and northeast (Figure 1) and the edge of the embayment might be related to the generation of scattered waves, we use 0–90° and 270–360° as azimuths of possible noise sources. We compute the average $\delta t/t$ variations from all station pairs with the azimuth in these ranges. In Figure 6, the average $\delta t/t$ variations are similar to each other, and the difference between them are very small compared to the maximum seasonal variations of the average $\delta t/t$. Hadziioannou et al. (2011) also observed that changes in noise directions do not influence the $\delta t/t$ measurements significantly. We conclude that the nonuniform distribution of noise sources has a small effect on the $\delta t/t$ variations.

The amplitude of the ambient noise usually shows seasonal variations (Stehly et al., 2006; Yang et al., 2007; Young, 1999). To investigate the velocity variation dependence on the seasonal changes of the amplitude of noise sources, we compare the $\delta t/t$ variations with the seasonal variations of the daily noise amplitude. We estimate hourly noise amplitude by averaging the absolute value of the original data in the passband of 0.3–2 Hz, and determine the daily noise amplitude by averaging over 24 hr. In Figure 7, we observe high amplitude from November to May and low amplitude from June to October, which is consistent with the generally observed high noise energy during winter in the Northern Hemisphere (Hillers et al., 2015; Liu et al., 2019; Young, 1999). We also observe high similarity between seasonal variation of the wind speed and average noise amplitude. Hillers et al. (2015) suggested the low-frequency (0.1–2 Hz) noise in the San Jacinto fault area can be excited by the atmosphere-ocean-lithosphere interactions. Thus, ambient noise from 0.3 to 2 Hz in the ME can be composed of oceanic microseisms (Langston et al., 2005, 2009; Liu, Langston, et al., 2018), induced surface waves at the basin edges (Kawase, 1996; Liu, Langston, et al., 2018; Liu et al., 2019), and wind. In Figure 7, we compare the variations of noise amplitude and $\delta t/t$ measurements from January to April and October to December, and observe high similarity between them. We also observe a small increase of $\delta t/t$ measurements with a large increase of noise amplitude in November (Figure 7). It is consistent with observation in previous section that wind speed changes are inversely correlated with the variation of $\delta v/v$ residual. Hillers et al. (2015) also proposed that changes in noise amplitude do not affect the velocity directly but can introduce a bias, a small increase or decrease, in the $\delta t/t$ measurements. Even if a decrease of noise amplitude from April to September can induce a small decrease of the $\delta t/t$ measurement, the decrease is

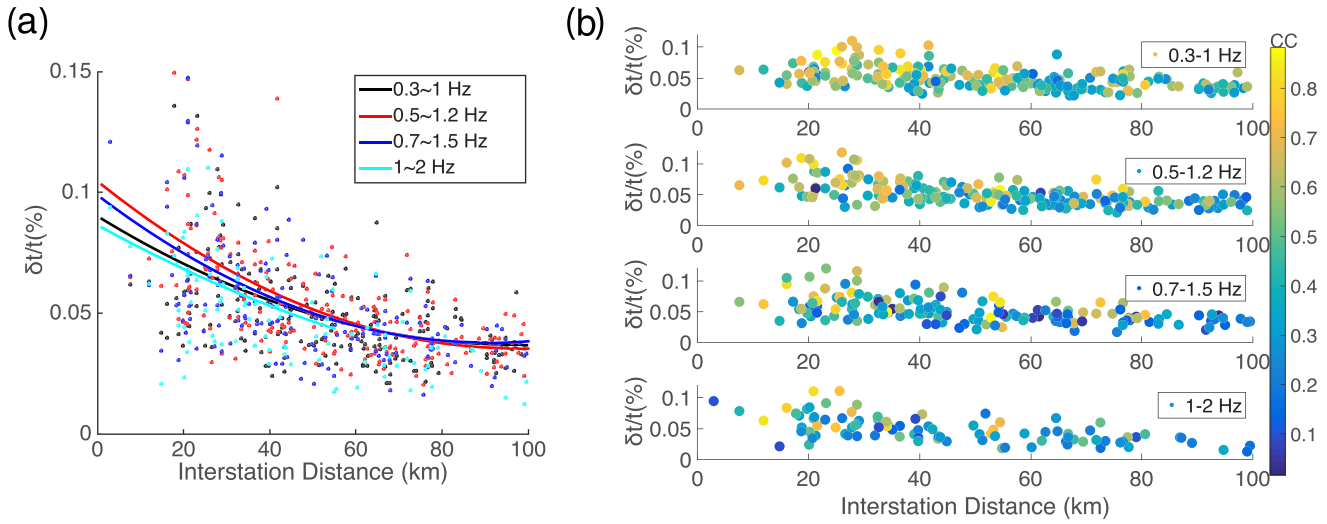

Figure 8. The $\delta t/t$ and correlation coefficient dependence on the interstation distance. (a) The maximum $\delta t/t$ variations decrease nonlinearly with the interstation distance. At close distance, $\delta t/t$ samples a small region and holds a wide range of values, which could be related to local sediment structure. At larger distances, $\delta t/t$ samples a large region so that it tends to stabilize to an average value. (b) Correlation coefficient dependence on the distance and frequency. The correlation coefficients are between water table fluctuation and $\delta t/t$ variations. High coefficients (>0.6) may be observed more often in the passband of 0.3–1 Hz than 1–2 Hz because high-frequency coherent noise attenuates faster than low-frequency noise.

relatively small compared to the $\delta t/t$ changes induced from the water table fluctuations. We conclude that the velocity variations are most likely related to the pore pressure changes in the crust or sediments, rather than changes due to the seasonal variations of the ambient noise amplitude.

3.4. Maximum $\delta t/t$ and Correlation Coefficient as a Function of Interstation Distance

In order to investigate propagation properties of noise in the sediments, we explore the relationship between $\delta t/t$ and interstation distance. The maximum $\delta t/t$ decreases nonlinearly with the increasing interstation distance as shown in Figure 8a. Because there are not enough station pairs with the interstation distance from 0 to 15 km, our analysis of the relationship between the $\delta t/t$ and distance is limited to 15–100 km. Meier et al. (2010) also observed that seasonal variations of $\delta t/t$ became weaker and finally disappeared when the interstation distance is greater than 60 km. They suggested that the vanishing of seasonal variation of $\delta t/t$ is due to absence of coherent noise in the coda window. At close distances, the $\delta t/t$ holds a wide range of values, which could be associated with greater localized variations in $\delta t/t$ in the local sediment structure. At larger distances, $\delta t/t$ variations tend to stabilize to a narrow range.

We compute correlation coefficients between normalized $\delta t/t$ variations and the normalized water table fluctuation over different distances, and investigate how the correlation coefficients depend on the interstation distance and frequency (Figure 8b). The correlation coefficients are independent of the interstation distance or frequency, but high coefficients (>0.6) are observed more often in the 0.3–1 Hz than 1–2 Hz passband because high-frequency coherent signals attenuate faster than low-frequency ones (Figure 8b).

4. Conclusions

We apply ambient noise correlation to 53 broadband stations which have continuous recordings in 2014 and analyze the seasonal variations of seismic velocity and determine how they correlate with the climatological parameters. We observe maximum $\delta t/t$ in May and June and minimum $\delta t/t$ in September and October relative to the average. At close distances, the maximum $\delta t/t$ holds a wide range of values, which could be associated with the local sediment structure. At larger distances, velocity variations tend to stabilize to an average value. The average $\delta t/t$ variations for station pairs with different azimuths are similar to each other, which suggests that the velocity variations do not depend on the azimuthal distribution of noise sources. Seasonal variations of noise amplitude might introduce a bias into the $\delta t/t$ estimation but the bias is small compared to the large velocity variations induced by the water table fluctuation.

The $\delta t/t$ correlates primarily with the normalized water table fluctuation. The $\delta v/v$ residuals correlate with air pressure in the short term and follow the trend of temperature in the long term. The $\delta t/t$ variation lags behind the water table fluctuation by about 20 days, which suggests the water diffusion effect is the dominant mechanism for the velocity change. We use a poroelastic model to estimate seasonal variations of $\delta v/v$ from 2010 to 2018. We find the optimal diffusion rate as 2.0 and 0.87 m^2/s through minimizing the squared residual and time lag between modeled and observed velocity changes, respectively. The optimal values are within the range of typical values inferred in previous studies (Rivet et al., 2015; Talwani et al., 2007; Wang et al., 2017). The correlation coefficients between the water table fluctuation and $\delta t/t$ are independent of the interstation distance and frequency, but more high coefficients (>0.6) are observed in the passband of 0.3–1 Hz than 1–2 Hz. One possible explanation could be that high-frequency coherent signals attenuate faster than low-frequency ones.

The results of the poroelastic model suggest that ambient noise cross correlations can be used to estimate the hydrological properties of sediments in other regions through minimizing residuals and time delay of the modeled and observed seismic velocity changes. This can provide an independent estimate of soil properties that are used in groundwater flow models.

Our results confirm that climatological variations play a role in determining the elastic properties of sediments in the Central and Eastern United States. Future studies should be completed in other intraplate regions to examine if similar behavior is found, which would provide additional ways to understand the physical mechanisms behind wave propagation and the temporal response of the crust to external forcing. In this manner, we can better determine if temporal velocity changes can be related to stress accumulation on faults due to tectonic loading and improve our ability to determine earthquake risk in intraplate fault regions.

Data Availability Statements

All ambient noise data are available in the IRIS DMC and requested through IRIS DMC web service (http://service.iris.edu/fdsnws). The ground water table data are provided from the USGS water resources information system (https://waterdata.usgs.gov/nwis/dv?), and the precipitation, temperature, atmospheric pressure, and the wind speed data are from the National Oceanic and Atomospheric Administration (NOAA) (https://www.ncdc.noaa.gov/cdo-web/search?datasetid=GHCND).

Acknowledgments

We thank Thomas Lecocq and an anonymous reviewer for constructive comments. This work was supported by funding from DOE Office of Basic Energy Science, Geoscience Program (Grant 89233218CNA000001) through Los Alamos National Laboratory and the Center for Earthquake Research and Information (CERI), University of Memphis.

References

Ben-Zion, Y., & Allam, A. A. (2013). Seasonal thermoelastic strain and postseismic effects in Parkfield borehole dilatometers. *Earth and Planetary Science Letters*, *379*, 120–126.

Ben-Zion, Y., & Leary, P. (1986). Thermoelastic strain in a half-space covered by unconsolidated material. *Bulletin of the Seismological Society of America*, *76*(5), 1447–1460.

Biot, M. A., & Willis, D. G. (1957). The elastic coefficients of the theory of consolidation. *Journal of Applied Mechanics*, *24*, 594–601.

Brekke, G. N. (1959). Wind pressures in various areas of the United States. National Bureau of Standardsra, 152.

Brenguier, F., Campillo, M., Hadziioannou, C., Shapiro, N. M., Nadeau, R. M., & Larose, E. (2008). Postseismic relaxation along the San Andreas fault at Parkfield from continuous seismological observations. *Science*, *321*(5895), 1478–1481.

Brenguier, F., Shapiro, N. M., Campillo, M., Ferrazzini, V., Duputel, Z., Coutant, O., & Nercessian, A.(2008). Towards forecasting volcanic eruptions using seismic noise. *Nature Geoscience*, *1*(2), 126.

Catchings, R. D. (1999). Regional *Vp*, *Vs*, *Vp*/*Vs*, and Poisson's ratios across earthquake source zones from Memphis, Tennessee, to St. Louis, Missouri. *Bulletin of the Seismological Society of America*, *89*(6), 1591–1605.

Clarke, D., Zaccarelli, L., Shapiro, N. M., & Brenguier, F. (2011). Assessment of resolution and accuracy of the Moving Window Cross Spectral technique for monitoring crustal temporal variations using ambient seismic noise. *Geophysical Journal International*, *186*(2), 867–882.

Clements, T., & Denolle, M. A. (2018). Tracking groundwater levels using the ambient seismic field. *Geophysical Research Letters*, *45*, 6459–6465. https://doi.org/10.1029/2018GL077706

D'Angelo, R. M., Winkler, K. W., & Johnson, D. L. (2008). Three wave mixing test of hyperelasticity in highly nonlinear solids: Sedimentary rocks. *The Journal of the Acoustical Society of America*, *123*(2), 622–639.

Dart, R. L. (1992). Catalog of pre-Cretaceous geologic drill-hole data from the upper Mississippi Embayment; a revision and update of open-file report 90-260: US Dept. of the Interior, US Geological Survey.

Dart, R. L., & Swolfs, H. S. (1998). Contour mapping of relic structures in the Precambrian basement of the Reelfoot rift, North American midcontinent. *Tectonics*, *17*(2), 235–249.

De Fazio, T. L., Aki, K., & Alba, J. (1973). Solid earth tide and observed change in the in situ seismic velocity. *Journal of Geophysical Research*, *78*(8), 1319–1322.

Derode, A., Larose, E., Campillo, M., & Fink, M. (2003). How to estimate the Green's function of a heterogeneous medium between two passive sensors? Application to acoustic waves. *Applied Physics Letters*, *83*(15), 3054–3056.

Dorman, J., & Smalley, R. (1994). Low-frequency seismic surface waves in the upper mississippi embayment. *Seismological Research Letters*, *65*(2), 137–148.

Duputel, Z., Ferrazzini, V., Brenguier, F., Shapiro, N., Campillo, M., & Nercessian, A. (2009). Real time monitoring of relative velocity changes using ambient seismic noise at the Piton de la Fournaise volcano (La Réunion) from January 2006 to June 2007. *Journal of Volcanology and Geothermal Research*, *184*(1-2), 164–173.

Froment, B., Campillo, M., Roux, P., Gouedard, P., Verdel, A., & Weaver, R. L. (2010). Estimation of the effect of nonisotropically distributed energy on the apparent arrival time in correlations. *Geophysics*, *75*(5), SA85–SA93.

Hadziioannou, C., Larose, E., Baig, A., Roux, P., & Campillo, M. (2011). Improving temporal resolution in ambient noise monitoring of seismic wave speed. *Journal of Geophysical Research*, *116*, B07304. https://doi.org/10.1029/2011JB008200

Hadziioannou, C., Larose, E., Coutant, O., Roux, P., & Campillo, M. (2009). Stability of monitoring weak changes in multiply scattering media with ambient noise correlation: Laboratory experiments. *The Journal of the Acoustical Society of America*, *125*(6), 3688–3695.

Hart, D. J. (2000). Laboratory measurements of poroelastic constants and flow parameters and some associated phenomena (P.h.D thesis), University of Wisconsin–Madison.

Hildenbrand, T. G., & Hendricks, J. D. (1995). Geophysical setting of the Reelfoot rift and relations between rift structures and the New Madrid seismic zone: United States Geological Survey.

Hillers, G., Ben-Zion, Y., Campillo, M., & Zigone, D. (2015). Seasonal variations of seismic velocities in the San Jacinto fault area observed with ambient seismic noise. *Geophysical Journal International*, *202*(2), 920–932.

Hillers, G., Retailleau, L., Campillo, M., Inbal, A., Ampuero, J.-P., & Nishimura, T. (2015). In situ observations of velocity changes in response to tidal deformation from analysis of the high-frequency ambient wavefield. *Journal of Geophysical Research: Solid Earth*, *120*, 210–225. https://doi.org/10.1002/2014JB011318

Hughes, D. S., & Kelly, J. L. (1953). Second-order elastic deformation of solids. *Physical review*, *92*(5), 1145.

Husen, S., Bachmann, C., & Giardini, D. (2007). Locally triggered seismicity in the central Swiss Alps following the large rainfall event of August 2005. *Geophysical Journal International*, *171*(3), 1126–1134.

Johnston, A. C., & Schweig, E. S. (1996). The enigma of the New Madrid earthquakes of 1811–1812. *Annual Review of Earth and Planetary Sciences*, *24*(1), 339–384.

Kawase, H. (1996). The cause of the damage belt in Kobe: The basin-edge effect, constructive interference of the direct *S*-wave with the basin-induced diffracted/Rayleigh waves. *Seismological Research Letters*, *67*(5), 25–34.

Langston, C. A., Bodin, P., Powell, C., Withers, M., Horton, S., & Mooney, W. (2005). Bulk sediment Q_p and Q_s in the Mississippi embayment, central United States. *Bulletin of the Seismological Society of America*, *95*(6), 2162–2179.

Langston, C. A., Chiu, S.-C. C., Lawrence, Z., Bodin, P., & Horton, S. (2009). Array observations of microseismic noise and the nature of H/V in the Mississippi embayment. *Bulletin of the Seismological Society of America*, *99*(5), 2893–2911.

Lecocq, T., Caudron, C., & Brenguier, F. (2014). MSNoise, a python package for monitoring seismic velocity changes using ambient seismic noise. *Seismological Research Letters*, *85*(3), 715–726.

Lecocq, T., Longuevergne, L., Pedersen, H. A., Brenguier, F., & Stammler, K. (2017). Monitoring ground water storage at mesoscale using seismic noise: 30 years of continuous observation and thermo-elastic and hydrological modeling. *Scientific Reports*, *7*(1), 1–16.

Li, Y.-G., Chen, P., Cochran, E. S., Vidale, J. E., & Burdette, T. (2006). Seismic evidence for rock damage and healing on the San Andreas fault associated with the 2004 *M* 6.0 Parkfield earthquake. *Bulletin of the Seismological Society of America*, *96*(4B), S349–S363.

Li, Y.-G., Vidale, J. E., Aki, K., Xu, F., & Burdette, T. (1998). Evidence of shallow fault zone strengthening after the 1992 *M*7. 5 Landers, California, earthquake. *Science*, *279*(5348), 217–219.

Li, Y.-G., Vidale, J. E., Day, S. M., Oglesby, D. D., & Cochran, E. (2003). Postseismic fault healing on the rupture zone of the 1999 *M* 7.1 Hector Mine, California, earthquake. *Bulletin of the Seismological Society of America*, *93*(2), 854–869.

Liu, C., Aslam, K., & Langston, C. A. (2019). Directionality of ambient noise in the Mississippi embayment. EarthArXiv. https://doi.org/10.31223/osf.io/5q8hx

Liu, Z., Huang, J., He, P., & Qi, J. (2018). Ambient noise monitoring of seismic velocity around the Longmenshan fault zone from 10 years of continuous observation. *Journal of Geophysical Research: Solid Earth*, *123*, 8979–8994. https://doi.org/10.1029/2018JB015986

Liu, C., Langston, C. A., Powell, C. A., & Cramer, C. H. (2018). Near surface to upper mantle velocity structure in the Mississippi embayment from ambient noise tomography. AGU Fall Meeting Abstracts.

Liu, C., Linde, A. T., & Sacks, I. S. (2009). Slow earthquakes triggered by typhoons. *Nature*, *459*(7248), 833.

Mao, S., Campillo, M., van der Hilst, R. D., Brenguier, F., Stehly, L., & Hillers, G. (2019). High temporal resolution monitoring of small variations in crustal strain by dense seismic arrays. *Geophysical Research Letters*, *46*, 128–137. https://doi.org/10.1029/2018GL079944

Meier, U., Shapiro, N. M., & Brenguier, F. (2010). Detecting seasonal variations in seismic velocities within Los Angeles basin from correlations of ambient seismic noise. *Geophysical Journal International*, *181*(2), 985–996.

Minato, S., Tsuji, T., Ohmi, S., & Matsuoka, T. (2012). Monitoring seismic velocity change caused by the 2011 Tohoku-Oki earthquake using ambient noise records. *Geophysical Research Letters*, *39*, L09309. https://doi.org/10.1029/2012GL051405

Murnaghan, F. D. (1951). *Finite deformation of an elastic solid*. New York: Wiley.

Nishimura, T., Uchida, N., Sato, H., Ohtake, M., Tanaka, S., & Hamaguchi, H. (2000). Temporal changes of the crustal structure associated with the *M*6.1 earthquake on September 3, 1998, and the volcanic activity of Mount Iwate, Japan. *Geophysical Research Letters*, *27*(2), 269–272.

Niu, F., Silver, P. G., Daley, T. M., Cheng, X., & Majer, E. L. (2008). Preseismic velocity changes observed from active source monitoring at the Parkfield SAFOD drill site. *Nature*, *454*(7201), 204.

Ohmi, S., Hirahara, K., Wada, H., & Ito, K. (2008). Temporal variations of crustal structure in the source region of the 2007 Noto Hanto earthquake, central Japan, with passive image interferometry. *Earth, Planets and Space*, *60*(10), 1069–1074.

Peng, Z., & Ben-Zion, Y. (2006). Temporal changes of shallow seismic velocity around the Karadere-Düzce branch of the north Anatolian fault and strong ground motion. *Pure and Applied Geophysics*, *163*(2-3), 567–600.

Poupinet, G., Ellsworth, W. L., & Frechet, J. (1984). Monitoring velocity variations in the crust using earthquake doublets: An application to the Calaveras Fault, California. *Journal of Geophysical Research*, *89*(B7), 5719–5731.

Rivet, D., Brenguier, F., & Cappa, F. (2015). Improved detection of preeruptive seismic velocity drops at the Piton de la Fournaise volcano. *Geophysical Research Letters*, *42*, 6332–6339. https://doi.org/10.1002/2015GL064835

Rubinstein, J. L., & Beroza, G. C. (2004a). Evidence for widespread nonlinear strong ground motion in the M_w 6.9 Loma Prieta earthquake. *Bulletin of the Seismological Society of America*, *94*(5), 1595–1608.

Rubinstein, J. L., & Beroza, G. C. (2004b). Nonlinear strong ground motion in the M_L 5.4 Chittenden earthquake: Evidence that preexisting damage increases susceptibility to further damage. *Geophysical research letters*, *31*, L23614. https://doi.org/10.1029/2004GL021357

Rubinstein, J. L., Uchida, N., & Beroza, G. C. (2007). Seismic velocity reductions caused by the 2003 Tokachi-Oki earthquake. *Journal of Geophysical Research*, *112*, B05315. https://doi.org/10.1029/2006JB004440

Sabra, K. G., Gerstoft, P., Roux, P., Kuperman, W. A., & Fehler, M. C. (2005). Surface wave tomography from microseisms in Southern California. *Geophysical Research Letters*, *32*, L14311. https://doi.org/10.1029/2005GL023155

Schaff, D. P., & Beroza, G. C. (2004). Coseismic and postseismic velocity changes measured by repeating earthquakes. *Journal of Geophysical Research*, *109*, B10302. https://doi.org/10.1029/2004JB003011

Sens-Schönfelder, C. (2008). Synchronizing seismic networks with ambient noise. *Geophysical Journal International*, *174*(3), 966–970.

Sens-Schönfelder, C., & Larose, E. (2008). Temporal changes in the lunar soil from correlation of diffuse vibrations. *Physical Review E*, *78*(4), 045,601.

Sens-Schönfelder, C., & Wegler, U. (2006). Passive image interferometry and seasonal variations of seismic velocities at Merapi Volcano, Indonesia. *Geophysical Research Letters*, *33*, L21302. https://doi.org/10.1029/2006GL027797

Shapiro, N. M., & Campillo, M. (2004). Emergence of broadband Rayleigh waves from correlations of the ambient seismic noise. *Geophysical Research Letters*, *31*, L07614. https://doi.org/10.1029/2004GL019491

Silver, P. G., Daley, T. M., Niu, F., & Majer, E. L. (2007). Active source monitoring of cross-well seismic travel time for stress-induced changes. *Bulletin of the Seismological Society of America*, *97*(1B), 281–293.

Stehly, L., Campillo, M., & Shapiro, N. M. (2006). A study of the seismic noise from its long-range correlation properties. *Journal of Geophysical Research*, *111*, B10306. https://doi.org/10.1029/2005JB004237

Stehly, L., Campillo, M., & Shapiro, N. M. (2007). Traveltime measurements from noise correlation: Stability and detection of instrumental time-shifts. *Geophysical Journal International*, *171*(1), 223–230.

Talwani, P., Chen, L., & Gahalaut, K. (2007). Seismogenic permeability, ks. *Journal of Geophysical Research*, *112*, B07309. https://doi.org/10.1029/2006JB004665

Tian, Y., & Ritzwoller, M. H. (2015). Directionality of ambient noise on the Juan de Fuca plate: Implications for source locations of the primary and secondary microseisms. *Geophysical Journal International*, *201*(1), 429–443.

Tsai, V. C. (2011). A model for seasonal changes in GPS positions and seismic wave speeds due to thermoelastic and hydrologic variations. *Journal of Geophysical Research*, *116*, B04404. https://doi.org/10.1029/2010JB008156

Wang, Q.-Y., Brenguier, F., Campillo, M., Lecointre, A., Takeda, T., & Aoki, Y. (2017). Seasonal crustal seismic velocity changes throughout Japan. *Journal of Geophysical Research: Solid Earth*, *122*, 7987–8002. https://doi.org/10.1002/2017JB014307

Wang, B., Yang, W., Wang, W., Yang, J., Li, X., & Ye, B. (2020). Diurnal and semidiurnal P-and S-wave velocity changes measured using an airgun source. *Journal of Geophysical Research: Solid Earth*, *125*, e2019JB018218. https://doi.org/10.1029/2019JB018218

Weaver, R., Froment, B., & Campillo, M. (2009). On the correlation of non-isotropically distributed ballistic scalar diffuse waves. *The Journal of the Acoustical Society of America*, *126*(4), 1817–1826.

Weaver, R. L., & Lobkis, O. I. (2001). Ultrasonics without a source: Thermal fluctuation correlations at Mhz frequencies. *Physical Review Letters*, *87*(13), 134,301.

Wegler, U., Lühr, B.-G., Snieder, R., & Ratdomopurbo, A. (2006). Increase of shear wave velocity before the 1998 eruption of Merapi volcano (Indonesia). *Geophysical Research Letters*, *33*, L09303. https://doi.org/10.1029/2006GL025928

Wegler, U., & Sens-Schönfelder, C. (2007). Fault zone monitoring with passive image interferometry. *Geophysical Journal International*, *168*(3), 1029–1033.

Wu, C., Delorey, A., Brenguier, F., Hadziioannou, C., Daub, E. G., & Johnson, P. (2016). Constraining depth range of s wave velocity decrease after large earthquakes near Parkfield, California. *Geophysical Research Letters*, *43*, 6129–6136. https://doi.org/10.1002/2016GL069145

Yamamura, K., Sano, O., Utada, H., Takei, Y., Nakao, S., & Fukao, Y. (2003). Long-term observation of in situ seismic velocity and attenuation. *Journal of Geophysical Research*, *108*(B6), 2317. https://doi.org/10.1002/jgrb.v108.b6

Yang, Y., Ritzwoller, M. H., Levshin, A. L., & Shapiro, N. M. (2007). Ambient noise Rayleigh wave tomography across Europe. *Geophysical Journal International*, *168*(1), 259–274.

Young, I. R. (1999). Seasonal variability of the global ocean wind and wave climate. *International Journal of Climatology: A Journal of the Royal Meteorological Society*, *19*(9), 931–950.

Zhan, Z., Tsai, V. C., & Clayton, R. W. (2013). Spurious velocity changes caused by temporal variations in ambient noise frequency content. *Geophysical Journal International*, *194*(3), 1574–1581.